CANCER BIOTHERAPY AND RADIOPHARMACEUTICALS
Volume 34, Number 5, 2019

DOI: 10.1089/cbr.2018.2616

^{89}Zr-DFO-Cetuximab as a Molecular Imaging Agent to Identify Cetuximab Resistance in Head and Neck Squamous Cell Carcinoma

Raquel Benedetto,[1] Adriana V.F. Massicano,[2] Bryant K. Crenshaw,[2] Renato Oliveira,[3] Rui M. Reis,[3] Elaine B. Araújo,[1] and Suzanne E. Lapi[2]

Abstract

Background: Despite the improvement in clinical outcomes for head and neck squamous cell carcinoma (HNSCC) as the result of cetuximab, patients may present with or develop resistance that increases tumor recurrence rates and limits clinical efficacy. Therefore, identifying those patients who are or become resistant is essential to tailor the best therapeutic approach.
Materials and Methods: Cetuximab was conjugated to p-NCS-Bz-DFO and labeled with ^{89}Zr. The resistance model was developed by treating FaDu cells with cetuximab. Western blotting (WB) and specific binding assays were performed to evaluate epidermal growth factor receptor (EGFR) expression and ^{89}Zr-DFO-cetuximab uptake in FaDu cetuximab-resistant (FCR) and FaDu cetuximab-sensitive (FCS) cells. Positron emission tomography imaging and biodistribution were conducted in NU/NU nude mice implanted with FCR or FCS cells.
Results: Cetuximab was successfully radiolabeled with ^{89}Zr (≥95%). Binding assays performed in FCR and FCS cells showed significantly lower ^{89}Zr-DFO-cetuximab uptake in FCR ($p < 0.0001$). WB suggests that the resistance mechanism is associated with EGFR downregulation ($p = 0.038$). This result is in agreement with the low uptake of ^{89}Zr-DFO-cetuximab in FCR cells. Tumor uptake of ^{89}Zr-DFO-cetuximab in FCR was significantly lower than FCS tumors ($p = 0.0340$).
Conclusions: In this work, the authors showed that ^{89}Zr-DFO-cetuximab is suitable for identification of EGFR downregulation *in vitro* and *in vivo*. This radiopharmaceutical may be useful for monitoring resistance in HNSCC patients during cetuximab therapy.

Keywords: cetuximab, EGFR, PET imaging, resistance, zirconium-89

Introduction

While progress in imaging techniques has led to improved diagnosis and staging in cancer patients, new techniques with improved specificity for receptors for targeted therapy are needed. These new imaging agents may help identify patients who would respond to (or are resistant to) targeted therapy.[1,2] As an example, development of new monoclonal antibodies (mAbs) has been an active area of research due to the success in therapeutic applications. These agents are specific against key molecular targets which are overexpressed or unique to tumor cells.[1,3]

The clinical value of mAbs is usually based on target-specific mechanisms that trigger a blockade of cell proliferation.[2,4] Several targets, such as B-lymphocyte antigen CD20, vascular endothelial growth factor (VEGF), and epidermal growth factor receptor (EGFR), have been successfully targeted in specific malignancies with effective mAbs.[1] Cetuximab is an IgG1 chimeric mAb against the EGFR, a tyrosine kinase receptor that plays an important role in cellular proliferation, DNA repair, and regulation responses to hypoxia.[5,6] This cell surface receptor is overexpressed in many types of cancer: nonsmall cell lung cancer, epithelial ovarian cancer, and in more than 90% of head and neck squamous cell carcinoma (HNSCC).[6]

[1]Instituto de Pesquisas Energéticas e Nucleares (IPEN), Sao Paulo, Brazil.
[2]Department of Radiology, University of Alabama at Birmingham (UAB), Birmingham, Alabama.
[3]Molecular Oncology Research Center, Barretos Cancer Hospital, Sao Paulo, Brazil.

Address correspondence to: Suzanne E. Lapi; Department of Radiology and Chemistry, University of Alabama at Birmingham, Wallace Tumor Institute 310F; 1824 6th Ave. South, Birmingham, AL 35233-3300
E-mail: **lapi@uab.edu**

Cetuximab was approved by the Food and Drug Administration (FDA) in 2004, as a single drug or in combination with chemotherapy for treatment of colorectal and HNSCC or in combination with external radiotherapy for HNSCC.[7] According to the World Health Organization, HNSCC is the fifth most common cancer worldwide, with an overall annual occurrence of 980,000 new cases. HNSCC patients have several options for therapy, including surgery, chemotherapy, radiotherapy, and targeted therapy, using mAbs. Despite clinical gains arising from use of cetuximab, patients may present inherent or acquired resistance, which increases tumor recurrence rates and limits clinical response.[8] The molecular heterogeneity of HNSCC has diverse implications in terms of possible mechanisms of either intrinsic or acquired resistance to EGFR-targeted inhibitors, several of these have been described, such as the activation of alternative signaling or the aberrance of the downstream pathways.[9–12] However, some patients with HNSCC whose tumors harbor EGFR mutations have benefitted from anti-EGFR immunotherapy.[13–15] Therefore, according to Brand et al., determining how to distinguish individuals sensitive to cetuximab is worthy of clinical investigation.[10]

The development of noninvasive imaging techniques using mAbs is a swiftly evolving field and a promising method to characterize the status of EGFR expressing tissue.[3,7] Imaging with radiolabeled cetuximab may be of use to evaluate potential treatment resistance and select patients who may respond well to antibody therapy. In addition, imaging using radiolabeled mAbs may enable a personalized medicine approach for targeted therapy.[5,7] The exceptional affinity, specificity, and selectivity of antibodies make them extraordinarily attractive vectors for tumor-targeted radiopharmaceuticals.[16] Radionuclides used for imaging should be selected to match the inherent properties of studied antibodies.[5]

Cetuximab has been labeled with different radionuclides for diagnosis: ^{99m}Tc ($t_{1/2}=6$ h)[17,18]; ^{68}Ga ($t_{1/2}=67.71$ min)[19]; ^{64}Cu ($t_{1/2}=12.7$ h)[20–24]; ^{124}I ($t_{1/2}=100.2$ h)[25–27]; ^{111}In ($t_{1/2}=67.2$ h)[7,28–33]; and ^{89}Zr ($t_{1/2}=78.4$ h).[16,34–47] mAbs have been labeled with γ-emitting radionuclides and imaged with a single-photon emission computed tomography camera.[17] Positron emission tomography (PET) for mAb imaging offers the potential of higher sensitivity and more accurate quantitation.[48,49] The introduction of PET with mAbs is an attractive novel option to improve diagnostic tumor characterization, because it combines the high sensitivity and resolution of a PET camera with the specificity of a mAb.[45,49] However, for a positron emitter to be appropriate for immuno-PET, it must meet certain requirements, including suitable decay characteristics and chemistry, which should allow facile, efficient, and stable coupling to mAbs.[49] Radionuclides with an ultrashort physical half-life might not be appropriate because of the inability to image at long time points, which is necessary due to the long circulation time of cetuximab with a biologic half-life about 63 h.[7]

The interest in positron-emitting radioisotopes with half-lives compatible with antibody imaging has led to an increase in interest in zirconium-89. ^{89}Zr is readily produced via the ^{89}Y(p,n) ^{89}Zr reaction on a cyclotron using a commercially available and 100% naturally abundant ^{89}Y target.[16,48] This radiometal displays highly desirable attributes as an imaging agent: a half-life that matches the pharmacokinetics of antibodies, well-developed radiolabeling chemistry, and a low positron energy (395.5 keV).[38,43] It is relevant to note that ^{89}Zr also emits a high energy, 909 keV γ-ray with a 99% branching ratio. Although this emission does not impact images acquired with the annihilation 511 keV photons, it does require extra attention with regard to transport, handling, and dosimetry. Despite this caveat, ultimately, ^{89}Zr not only has a more satisfactory half-life for imaging with antibodies than ^{64}Cu but can also provide higher resolution images than ^{124}I.[40,41] Moreover, ^{89}Zr is also less expensive to produce, and it residualizes in tumors more effectively than its radioiodine counterpart.[16,40,49] Regarding the dosimetry concern to the patient, several clinical trials have demonstrated the feasibility and safety of ^{89}Zr-radiolabeled antibodies (administered activities of 37–74 MBq).[38,40,46] Due to the numerous advantages of ^{89}Zr-based antibody imaging, its clinical potential is advancing, leading to an exciting strategy to improve diagnostic imaging and to assess target expression.[34,40,42,43,50]

The potential of EGFR as a target for both imaging and therapy has been an active area of investigation. Cetuximab, in particular, has been the focus of a number of imaging studies for the purpose of monitoring disease, EGFR expression, patient selection or performing dosimetry calculations for targeted therapy trials.[51] In this work, the authors conducted proof-of-principle studies in animal models to assess the use of ^{89}Zr-DFO-cetuximab as a molecular imaging agent to monitor developed resistance in HNSCC during therapy with cetuximab.

Materials and Methods

Antibodies and reagents

The production of ^{89}Zr-oxalate was carried out in house (University of Alabama at Birmingham [UAB] Cyclotron Facility) from the ^{89}Y(p,n)^{89}Zr reaction using ^{89}Y sputtered targets as described previously.[52] Cetuximab (Erbitux®; Bristol-Myers Squibb) was purchased from Merck (Darmstadt, Germany). Anti-EGFR (EP384; ab52894) was purchased from Abcam (Cambridge, MA); anti-β actin (sc-47778 HRP) and goat anti-rabbit IgG-HRP (sc-2054) antibodies for Western blotting (WB) were purchased from Santa Cruz Biotechnology (Dallas, TX). Desferrioxamine-p-benzyl-isothiocyanate (DFO-Bz-NCS) was purchased from Macrocyclics (Dallas, TX). Dimethyl sulfoxide (DMSO) and sodium carbonate were purchased from Sigma-Aldrich (St. Louis, MO). HEPES was purchased from ACROS Organic (Fair Lawn, NJ). All other chemicals were purchased from Fisher Scientific (Hampton, NH) unless stated otherwise.

Cell lines and development of cetuximab resistance

The FaDu human squamous carcinoma cell line was purchased from American Type Culture Collection (ATCC) and cultivated in Iscove's Modified Dulbecco's Medium (IMDM) with 10% fetal bovine serum (FBS) and gentamycin (50 mg/mL) in a humidified incubator with 5% CO_2 at 37°C. All other reagents for cell culture were purchased from Gibco® Life Technologies (Grand Island, NY).

To develop acquired resistance, FaDu cells were kept in culture with fresh medium containing 0.2 mg of cetuximab added twice a week for 7 months[53] (Supplementary Fig. S1). To confirm resistance, a specific binding assay was performed monthly as described below. Three days prior the specific binding assay, the medium containing cetuximab was removed, the cells were washed two times with phosphate-buffered saline (PBS), trypsinized and plated into a 12-well plate with fresh medium without cetuximab. This procedure was performed to avoid cetuximab interference in the specific binding assay.

Once the cells became resistant, the cetuximab was removed from the culture medium, and the cells were split several times to conclude the *in vivo* experiments.

Preparation of ^{89}Zr-DFO-cetuximab

Cetuximab was conjugated to DFO-Bz-NCS and labeled with ^{89}Zr-oxalate according to previous methods.[25,30] In brief, fivefold molar excess of DFO-Bz-NCS dissolved in DMSO was conjugated to cetuximab in 0.1 M sodium carbonate buffer (pH 9) at 37°C for 1 h. After conjugation, excess DFO was removed via Zeba spin desalting columns (40 kDa Molecular Weight Cut-Off; Thermo Scientific, Rockford, IL) using 1 M HEPES buffer pH 7.1–7.3 as eluent. The final concentration of protein was determined using a bicinchoninic acid (BCA) assay (Thermo Scientific). The purified DFO-cetuximab was labeled with neutralized ^{89}Zr-oxalate (0.148 MBq/μg) at 37°C for 1 h. The resulting ^{89}Zr-DFO-cetuximab was purified using desalting columns and the radiochemical purity was determined by instant thin-layer chromatography using 50 mM DTPA as the developing solution.

In vitro-*specific cell binding*

The specific binding of ^{89}Zr-DFO-cetuximab was assessed in FaDu cetuximab-sensitive (FCS) and FaDu cetuximab-resistant (FCR) cells *in vitro*. Cells (1×10^5) were plated in a 12-well plate 48 h before the experiment and kept in culture as described above. On the day of the experiment, they were incubated with ^{89}Zr-DFO-cetuximab (5.5 nM; 0.12 MBq/mL in IMDM, 1% FBS) alone (total binding) or in presence of cold cetuximab (2.75 μM in IMDM or Dulbecco's modified Eagle's medium [DMEM] 1% FBS; competitive binding) for 3 h in a humidified incubator with 5% CO_2 at 37°C. Cells were washed with PBS, trypsinized, and assayed in a gamma counter (Wizard^2; Perkin Elmer, Waltham, MA). The percentage of ^{89}Zr-DFO-cetuximab bound to cells in presence or absence of competitor was calculated and corrected for protein concentration.

Western blotting

FCS and FCR cells were lysed with RIPA buffer (Alfa Aesar) and the concentration in the extracted lysates was measured by BCA assay. Proteins (20 μg) were loaded onto 7.5% Mini-PROTEAN TGX Stain-Free precast gels (Bio-Rad, Hercules, CA) in Tris/Glycin/SDS buffer for electrophoresis. Following electrophoresis, the proteins were transferred onto PVDF membranes gels (Bio-Rad) and blocked with nonfat dry milk (NFDM) diluted in PBST at 3% concentration for 1 h at room temperature. The membranes were incubated with anti-EGFR primary antibody (1:2000 in 3% NFDM) overnight at 4°C. After the incubation, membranes were washed and incubated with goat anti-rabbit HRP-conjugated anti-rabbit antibody (50 ng/mL in 3% NFDM) and anti-β actin (100 ng/mL in 3% NFDM) for 1 h at room temperature. After three to five washing cycles with PBST, the membranes were incubated with a chemiluminescent WB detection reagent (ECL Select, GE Healthcare, Chicago, IL) according to manufacturer's instructions and read using a ChemiDoc XRS+ imager (Bio-Rad). The EGFR bands were normalized by the amount of protein loaded (β-actin band) using Image software (National Institutes of Health, Bethesda, MD).

Fluorescent immunohistochemistry technique

Approximately 2×10^4 of both cell lines (FCS and FCR) were seeded on Falcon™ Chambered Cell Culture Slides overnight. The cell lines were washed three times with ice cold PBS, and with paraformaldehyde solution 4% for 10 min at room temperature. After fixation step, slides were washed three times in PBS and then permeabilized with Triton-X solution 0.25% (Sigma-Aldrich) in PBS for 10 min. Unspecific protein block was performed using Novocastra Protein Block solution (Leica Biosystems, Buffalo Grove, IL) for 30 min. The cells were incubated with anti-EGFR (31G7) ready to use (Invitrogen, Carlsbad, CA) overnight. Cells were washed three times with PBS and incubated in Alexa488-conjugated anti-mouse secondary antibody (Molecular Probes) at 1:1000 dilution for 1 h at room temperature. Nuclear counterstain was carried out with DAPI as a mounting reagent (Molecular Probes). The fluorescence microscopy images were conducted using the IN Cell Analyzer 2200 (GE Healthcare).

Animal studies

All animal experiments were performed with the approval of the Institutional Animal Care and Use Committee of the UAB.

Five-week old female NU/NU nude mice (Charles River, Wilmington, MA) were subcutaneously implanted with 5×10^5 FCR or FCS cells (four mice for each group). Tumors were allowed to grow for 2 weeks and mice were injected via tail vein with 2.22 MBq of ^{89}Zr-DFO-cetuximab (corresponding to 15 μg of cetuximab). After 3- and 5-d postinjection (p.i.), mice were imaged using a GNEXT small animal PET/computed tomography (CT; Sofie Biosciences, Culver City, CA). Immediately after imaging, mice were euthanized; tumors and select organs were collected, weighed, and analyzed in a gamma counter to measure radioactivity. The *in vivo* study design is shown in Figure 1.

Statistical analysis

For simple comparison, the student *t*-test was used. For multiple comparisons, one-way analysis of variance was performed followed by group comparisons using the Bonferroni method to control multiple comparisons. Statistical analysis was performed using GraphPad Prism version 7.04 (GraphPad Software, Inc., La Jolla, CA).

The results are expressed as mean ± standard error of the mean. Differences were regarded as statistically significant for $p<0.05$.

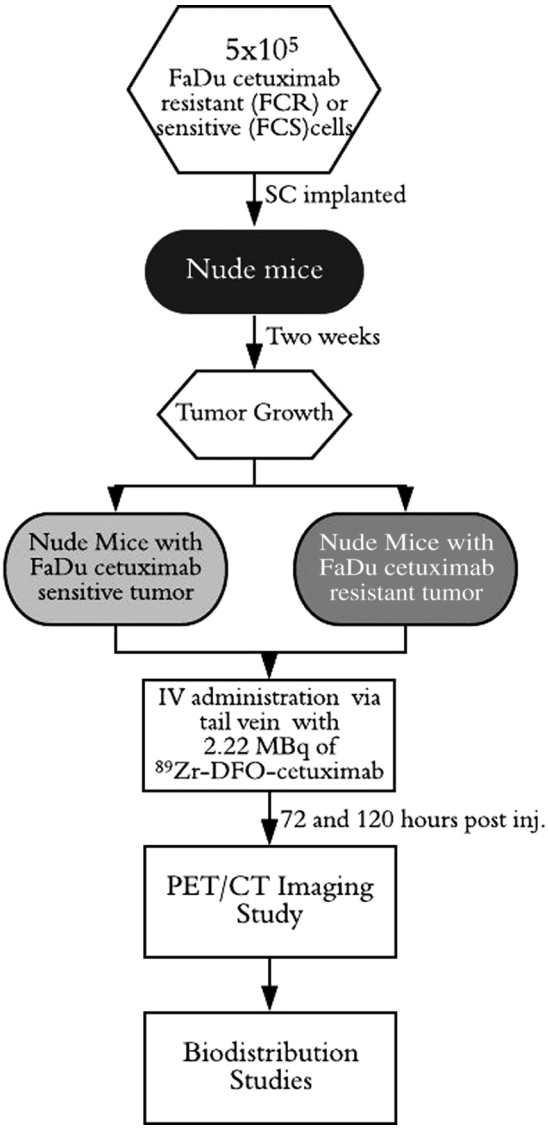

FIG. 1. Schematic representation of the *in vivo* study in NU/NU nude mice.

Results

^{89}Zr-DFO-cetuximab: radiochemical yield

^{89}Zr-DFO-cetuximab was produced with ≥95% radiochemical yield and specific activity of 0.148 MBq/μg.

Specific cell-binding studies of ^{89}Zr-DFO-cetuximab in vitro

The specificity of ^{89}Zr-DFO-cetuximab was investigated *in vitro* by comparing its binding in FCS and FCR cells (Fig. 2). Cell uptake studies demonstrated significant lower uptake of ^{89}Zr-DFO-cetuximab in FCR cells ($p<0.0001$). This is feasible to observe in total binding assay, since the percentage uptake per ng of protein was higher by six times in FCS cells when compared to FCR cells.

Quantification of in vitro *EGFR expression*

EGFR expression on cell lines was assessed by WB (Fig. 3) in FCR and FCS cells. FCS presented significantly higher *in vitro* EGFR expression (EGFR-to-actin ratio: 1.049 ± 0.353) than FCR (EGFR-to-actin ratio: 0.476 ± 0.126) which suggests EGFR downregulation in FCR ($p=0.038$). WB results imply that cetuximab induces resistance by EGFR downregulation in FaDu cells, and these outcomes corroborate with other studies previously published[54,55] (Supplementary Fig. S2).

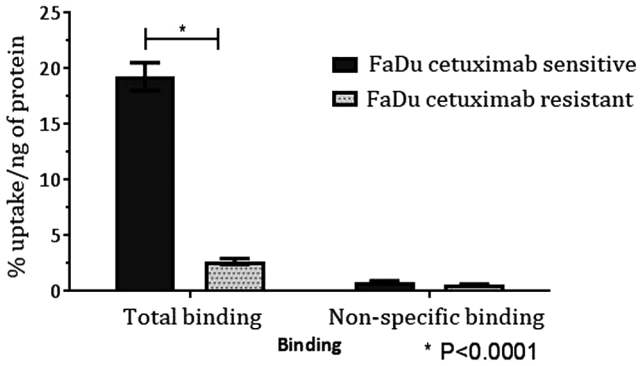

FIG. 2. *In vitro* cell uptake assay of ^{89}Zr-DFO-cetuximab uptake in FCS and FCR cells. FCR, FaDu cetuximab resistant; FCS, FaDu cetuximab sensitive.

Cell uptake studies demonstrated a correlation between EGFR expression *in vitro* and ^{89}Zr-DFO-cetuximab uptake. This result is consistent with the low uptake of ^{89}Zr-DFO-cetuximab in FCR cells.

Fluorescent immunohistochemistry technique

The immunofluorescence assay was performed to access EGFR localization and to detect a fluorescent labeling of

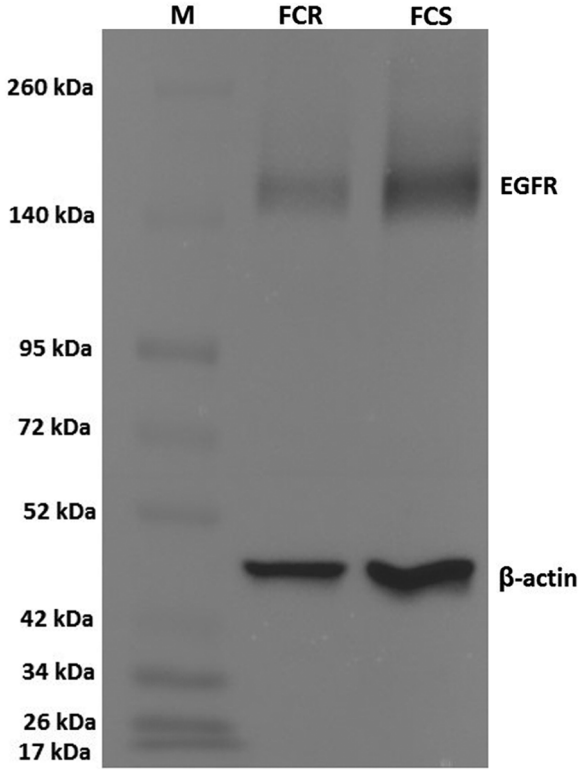

FIG. 3. Representative Western blotting of FCS and FCR cells. M, molecular weight marker.

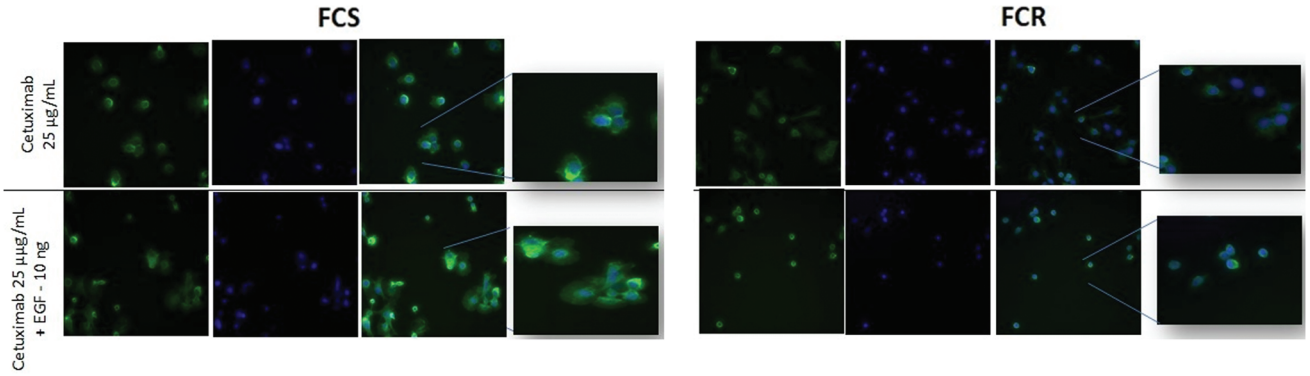

FIG. 4. Comparative fluorescent immunohistochemistry assay in FCS and FCR cells to access EGFR localization. EGFR, epidermal growth factor receptor. Color images are available online.

EGFR in FaDu sensitive cell line (FCS). Higher levels of membranous and cytoplasmic EGFR in FCS were observed when compared with the FCR (Fig. 4). Both cell lines were stimulated with EGF, and a difference in nuclear EGFR expression levels was detected, with the FaDu resistance cell line showing an exclusive nuclear labeling.

In vivo *uptake of ^{89}Zr-DFO-cetuximab: imaging study*

To evaluate the potential of ^{89}Zr-DFO-cetuximab as an imaging agent, and to compare the uptake of ^{89}Zr-DFO-cetuximab in resistant cells, imaging studies in mice bearing FCR or FCS xenografts were performed.

The tumor model was developed without the need for exogenous stimuli, and fast tumor growth was observed. After 2 weeks, FCR group present a tumor size of $63.07 \pm 7.25\,mm^3$ and FCS $296.7 \pm 6.71\,mm^3$.

The *in vivo* uptake of ^{89}Zr-DFO-cetuximab was assessed by performing PET/CT at 3 and 5 d p.i. of 2.22 MBq of ^{89}Zr-DFO-cetuximab in tumor-bearing mice (Fig. 5A, B). A clear accumulation of ^{89}Zr-DFO-cetuximab was found in the cetuximab sensitive tumors (FCS). FCS tumors showed higher mean standard updated value (0.26 ± 0.05; 3 d p.i.) compared with FCR tumors (0.13 ± 0.01; 3 d p.i), with a significant difference between the groups ($p < 0.05$). The radiotracer uptake was also observed in normal tissues such as the liver, likely due to hepatobiliary clearance of the antibody.[44]

Biodistribution studies

Biodistribution studies with ^{89}Zr-DFO-cetuximab were performed in NU/NU nude mice bearing FCS and FCR tumors at 3 and 5 d p.i. ^{89}Zr-DFO-cetuximab had similar biodistribution profile in normal organs of mice implanted with both cell lines (Fig. 6) ($p > 0.05$).

For the FCS group, the circulating levels of ^{89}Zr-DFO-cetuximab in the blood declined from $4.93\% \pm 3.03\%$ injected dose (ID)/g at 3 d p.i. to $0.57\% \pm 0.26\%$ ID/g at 5 d p.i. ($p = 0.0215$). Spleen uptake was $3.98\% \pm 0.78\%$ ID/g and $3.66\% \pm 0.93\%$ ID/g at 3 and 5 d p.i., respectively ($p > 0.05$). Liver accumulation of ^{89}Zr-DFO-cetuximab was $8.18\% \pm 2.59\%$ ID/g at 3 d p.i. and declined to $6.75\% \pm 0.69\%$ ID/g at 5 d p.i. ($p > 0.05$). Notable uptake was also found in the kidney ($3.08\% \pm 0.72\%$ ID/g and $2.341\% \pm 0.24\%$ ID/g at 3 and 5 d p.i., respectively ($p > 0.05$). Bone uptake was $6.70\% \pm 2.38\%$ ID/g at 3 d and $10.32\% \pm 3.10\%$ ID/g at 5 d p.i. ($p > 0.05$).

For the FCR group, the circulating levels of ^{89}Zr-DFO-cetuximab in the blood declined from $2.57\% \pm 3.84\%$ ID/g at 3 d p.i to $1.88\% \pm 2.12\%$ ID/g at 5 d p.i. ($p > 0.05$). Spleen uptake was $7.06\% \pm 2.50\%$ ID/g and $4.82\% \pm 3.50\%$ ID/g at 3 and 5 d p.i., respectively ($p > 0.05$). Liver accumulation of ^{89}Zr-DFO-cetuximab was $10.94\% \pm 2.35\%$ ID/g at 3 d p.i. and declined to $7.13\% \pm 2.07\%$ ID/g at 5 d p.i. ($p > 0.05$).

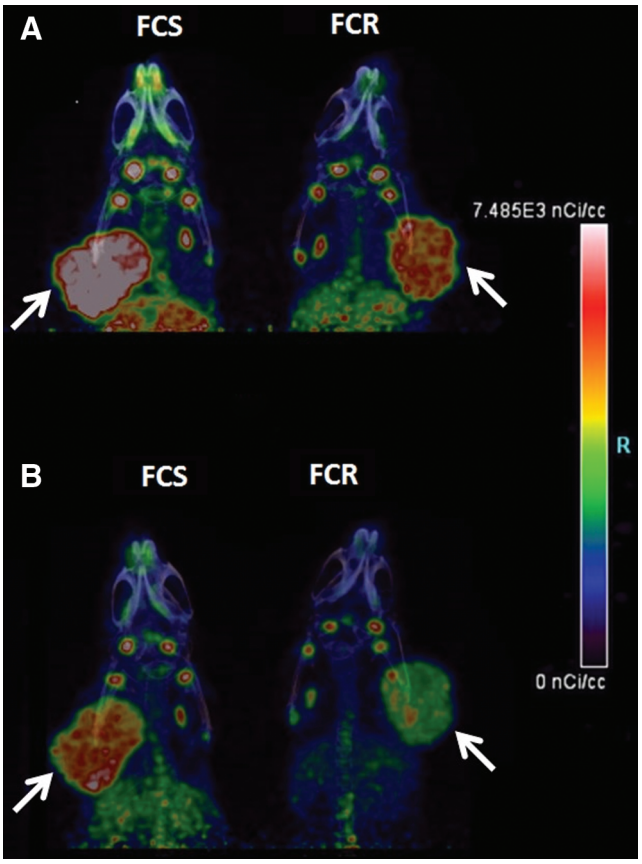

FIG. 5. Representative small-animal PET images **(A)** 3 d p.i. and **(B)** 5 d p.i. of ^{89}Zr-DFO-cetuximab in mice bearing FCS and FCR tumors. *White arrows* indicate the tumors. PET, positron emission tomography; p.i., postinjection. Color images are available online.

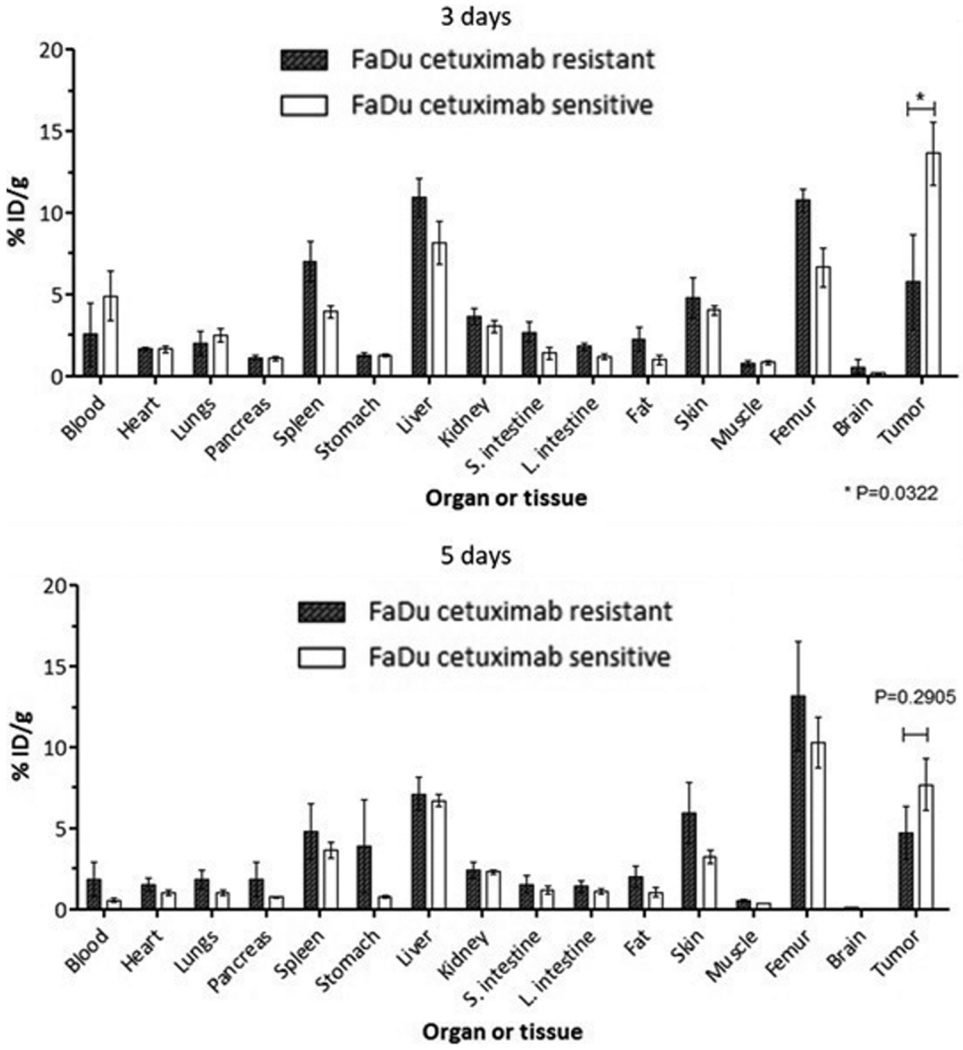

FIG. 6. Biodistribution data of ^{89}Zr-DFO-cetuximab in FCS and FCR xenograft models at 3 and 5 d p.i. Data are expressed as percent injected dose per gram ± standard deviation, $n=4$ for each time point.

Bone uptake was 10.79% ± 1.41% ID/g at 3 d and 13.21% ± 6.73% ID/g at 5 d p.i. ($p>0.05$). Tumor uptake of ^{89}Zr-DFO-cetuximab in FCS group (13.66% ± 3.80% ID/g) was significantly higher ($p=0.0322$) than FCR group (5.78% ± 5.09% ID/g) at 3 d p.i.

To assess the imaging potential of ^{89}Zr-DFO-cetuximab, the tumor-to-blood (T/B), tumor-to-liver (T/L), and tumor-to-femur (T/F) ratios were evaluated. As shown in Figure 7, a decreasing blood uptake were found in FCS group ($p=0.0215$), resulting in larger T/B ratios with time for the EGFR-positive tumors (Fig. 7). The mean tumor-to-mean blood ratio for FCS increased substantially after 5 d p.i. (13.56). The FCS group showed a significantly greater mean T/B ratio than FCR group at 5 d p.i. ($p<0.01$).

The T/L ratio was higher in the FCS group (1.67). Similarly, the FCS group presented a higher T/F ratio than FCR group (2.04 compared to 0.54, considering 3 d p.i.). However, no significant change in mean T/L and T/F ratios was observed as a function of time in both groups ($p>0.05$).

Discussion

The EGFR is highly expressed in a significant number of human malignancies, and its expression is associated with tumor aggressiveness and overall treatment resistance.[5–7] Discerning a patient's EGFR mutation status and the mechanism of acquired resistance is critical for effective disease management. Resistance most often arises through secondary mutations in EGFR, which account for 50% of the resistance mechanisms.[56] Studies have revealed that

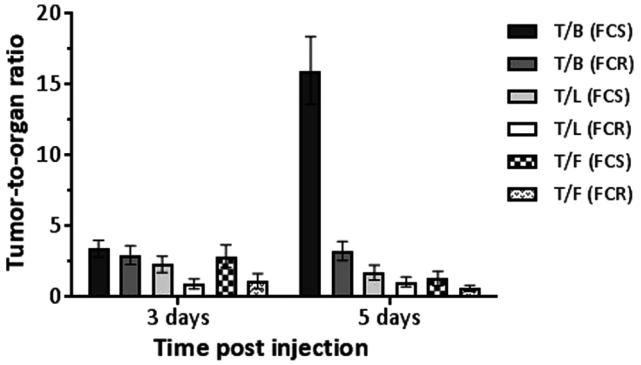

FIG. 7. T/B, T/L and T/F ratios of injected ^{89}Zr-DFO-cetuximab in mice bearing FCS and FCR tumor xenografts at 3 and 5 d p.i. Data are expressed as percent injected dose per gram (or cm^3) ± standard deviation, $n=4$ for each time point. T/B, tumor-to-blood; T/F, tumor-to-femur; T/L, tumor-to-liver.

downregulation of EGFR levels in lung cancer patient has a clinically relevant impact because these patients, with this mode of resistance, may not benefit from second- or third-generation EGFR-targeted TKIs.[57,58] Activation of MAPK8 has been previously reported as a potential bypass mechanism in lung cancer cell lines that are addicted to EGFR.[58] The use of noninvasive imaging techniques to identify cetuximab resistance profile can motivate improved patient theranostics and may ultimately lead to new treatment options.

Thus, the development of methods that can distinguish individuals sensitive to the EGFR-targeting antibody, cetuximab, may help to tailor the best therapeutic approach for each patient. Noninvasive quantification of cetuximab uptake could provide important diagnostic information for patient selection and therapy evaluation. For this study, ^{89}Zr-DFO-cetuximab was proposed as a molecular imaging agent to monitor resistance in HNSCC during therapy with cetuximab.

In this study, to reproduce the resistance mechanism of tumor cells to anti-EGFR therapy, a cetuximab-resistant cell line was developed, according to prior experiments conducted of the Oncology Research Center of the Hospital de Cancer de Barretos/Brazil.[53] The authors' findings illustrate that ^{89}Zr-DFO-cetuximab was able to differentiate between tumors sensitive and resistant to cetuximab. The *in vitro* and *in vivo* studies suggest a correlation between EGFR expression and ^{89}Zr-DFO-cetuximab uptake, resulting in low accumulation of the tracer in FCR cells.

EGFR expression quantification (assessed through WB) and *in vitro* cell studies and analysis demonstrated a correlation between EGFR expression and ^{89}Zr-DFO-cetuximab uptake (Figs. 2 and 3). *In vivo* studies were performed in mice bearing FCR or FCS xenografts. Similar to *in vitro* results, a correlation was observed between EGFR expression and tumor uptake of ^{89}Zr-DFO-cetuximab by small animal PET/CT imaging as shown in Figure 5. Benedetto[59] previously performed the blocking study, and the small animal PET/CT images have revealed a reduction in uptake profile for ''blocking'' group (with an excess of unlabeling cetuximab) and an intense ^{89}Zr-DFO-cetuximab uptake in FCS for ''non-blocking'' group, that illustrated the *in vivo* radioimmunoconjugate specificity. A higher level of radiotracer accumulation was observed in the FCS compared with FCR tumors. Nonuniform tumor growth rate may have contributed to the observed tumor uptake difference between FCS and FCR groups at 5 d postinjection. FCS tumors grew faster than FCR, in this sense, the tumor size might have interfered in this result.

Diversified approaches have been evaluated for the EGFR imaging. Anti-EGFR mAbs radiolabeled with ^{111}In, ^{64}Cu, ^{124}I, and ^{89}Zr have demonstrated specificity, however, limitations were observed in some of these studies, due to the type of emission or physical half-life of the radionuclide.[25,34,45,49] PET technology provides better resolution, however, maintenance of the antibody's *in vivo* binding and biodistribution characteristics is imperative, while the physical half-life ($t_{1/2}$) of the positron emitter should be compatible with the time needed for a mAb to achieve optimal tumor-to-nontumor ratios (typically 2.5 d).[7,49]

Cetuximab has been previously labeled with ^{64}Cu and has proved promising in preclinical investigations, although the ^{64}Cu physical half-life may be somewhat short for clinical imaging studies.[16] The half-lives of longer-lived positron emitters such as ^{124}I and ^{89}Zr have a much closer match with the biologic half-life of most intact antibodies.[41] Moreover, ^{64}Cu had a high liver uptake, ranging from 15% to 47% ID/g.[60] In the current study, the liver uptake was low when compared to the studies performed with ^{64}Cu,[60] probably due to the fact that ^{89}Zr is relatively bioinert compared to copper, and it may be less likely to react with the liver proteins. The liver uptake values observed in this study are in close agreement with Aerts et al., in previous preclinical work with ^{89}Zr-labeled cetuximab[44] and with England, who recently reported similar liver uptake values with ^{89}Zr-radiolabeled antibodies (8.49 ± 0.79% ID/g).[61]

The renal uptake observed is likely related to liver accumulation, suggesting that the radiotracer undergoes a hepatic metabolism and subsequent metabolites are eliminated through the urine.[45,61] Bile secretion is an important route of IgA clearance, but not significant for IgG, which explains the low uptake of ^{89}Zr-DFO-cetuximab in the intestines.[40,45] The high uptake in bone is expected since zirconium is a bone seeker.[43] The release of osteophilic Zr^{4+} *in vivo* leads to accumulation of the cation in the bone. In the comparative studies, Perk et al.[45] reported lower stability of the ^{89}Zr-DFO complex compared to the ^{88}Y- and ^{177}Lu-DOTA complexes, which was reflected in a significantly higher bone accumulation of ^{89}Zr compared to ^{88}Y and ^{177}Lu. In this study, the percent ID/g, 3 d p.i. (for FCS), was lower than 7%, and this bone uptake did not compromise the resulting image quality (Fig. 6).

The advances in noninvasive diagnostic methods of the past decade are showing signs of bringing developments in therapy.[43] Diagnostic information can assist in the selection of patients, and it can potentially predict the risk-benefit balance of a planned therapy with radionuclides through the dosimetric analysis.[50,51] In addition, the imaging data can aid with evaluation of the therapeutic response to a particular treatment and can guide the planning and therapeutic administration.[49] Therefore, ^{89}Zr-DFO-cetuximab may be used to noninvasively examine uptake of cetuximab into the tumor, thus allowing selection of patients who are or become resistant to anti-EGFR immunotherapy. In this regard, identification of these patients who can potentially benefit from cetuximab treatment is essential to tailor the best therapeutic approach.

Conclusions

In this work, ^{89}Zr-DFO-cetuximab was produced with high radiochemical yield for use in *in vitro* and *in vivo* studies. This study has demonstrated that cetuximab uptake in tumors can be assessed by PET using ^{89}Zr-labeled cetuximab, which corroborates the cetuximab resistance of HNSCC due to EGFR downregulation. In conclusion, ^{89}Zr-DFO-cetuximab is a suitable radiopharmaceutical to identify these downregulation *in vitro* and *in vivo* models. This radiopharmaceutical may be useful for monitoring resistance in HNSCC patients during therapy with cetuximab; therefore, future clinical studies should be investigated.

Acknowledgments

The authors thank Dr. Lapi's team, especially Cyclotron Facility group, for all the support and assistance in the production of ^{89}Zr and the small animal imaging team for assistance with the preclinical studies. The UAB Small Animal Imaging Shared Facility is supported by NIH grant P30CA013148 awarded to the UAB Comprehensive Cancer Center.

Authors' Contributions

R.B.—Conception: constructing the idea for research and article; Design: planning methodology to reach the conclusion; Analysis and Interpretation: interpretation and presentation of the results; Data Processing: taking responsibility in data management and reporting; Literature Review; Writer: taking responsibility in the construction of the article. A.V.F.M.—Conception: constructing the idea for article; Design: planning methodology to reach the conclusion; Analysis and Interpretation: interpretation and presentation of the results; Data Collection/Processing: taking responsibility in execution of the experiments; writer; review. B.K.C.—Data Collection: execution of the experiments; Review: reviewing the article grammar. R.O.—Conception: constructing the idea for the development of cetuximab resistance cell model. R.M.R.—Conception: constructing the idea for the development of cetuximab resistance cell model; Review: reviewing the article before submission. E.B.A.—Conception: constructing the idea for research; Critical Review: reviewing the article before submission. S.E.L.—Conception: constructing the idea for article; Critical Review: reviewing the article before submission.

Disclosure Statement

The authors declared no potential conflicts of interest with respect to the research, authorship, and/or publication of this article.

Supplementary Material

Supplementary Figure S1
Supplementary Figure S2

References

1. Strome SE, Sausville EA, Mann D. A mechanistic perspective of monoclonal antibodies in cancer therapy beyond target-related effects. Oncologist 2007;12:1084.
2. Lieber M. Antibody diversity: A link between switching and hypermutation. Curr Biol 2000;10:798.
3. Wright BD, Lapi SE. Designing the magic bullet? The advancement of immuno-PET into clinical use. J Nucl Med 2013;54:1171.
4. McCarron PA, Olwill SA, Marouf WM, et al. Antibody conjugates and therapeutic strategies. Mol Interv 2005;5:368.
5. Hoeben BA, Molkenboer-Kuenen JDM, Oyen WJG, et al. Radiolabeled cetuximab: Dose optimization for epidermal growth factor recept or imaging in a head-and-neck squamous cell carcinoma model. Int J Cancer 2011;129:870.
6. Wiechec E, Hansson T, Alexandersson L, et al. Hypoxia mediates differential response to anti-EGFR therapy in HNSCC cells. Int J Mol Sci 2017;18:943.
7. Lövqvist A, Humm JL, Sheikh A, et al. PET imaging of 86Y-labeled anti-Lewis Y monoclonal antibodies in a nude mouse model: comparison between 86Y and 111 in radiolabels. J Nucl Med 2001;42:1281–1287.
8. Lubner SJ. Primary and acquired resistance to biologic therapies in gastrointestinal cancers. J Gastrointest Oncol 2017;3:499.
9. Morgillo F, Della Corte CM, Fasano M, et al. Mechanisms of resistance to EGFR-targeted drugs: Lung cancer. ESMO Open 2016;1:1.
10. Brand TM, Lida M, Wheeler DL. Molecular mechanisms of resistance to the EGFR monoclonal antibody cetuximab. Cancer Biol Ther 2011;9:777.
11. Lievre A, Bachet JB, Le Corre D, et al. KRAS mutation status is predictive of response to cetuximab therapy in colorectal cancer. Cancer Res 2006;66:3992.
12. Di Fiore F, Blanchard F, Charbonnier F, et al. Clinical relevance of KRAS mutation detection in metastatic colorectal cancer treated by Cetuximab plus chemotherapy. Br J Cancer 2017;96:1166.
13. De Roock W, Piessevaux H, De Shutter J, et al. KRAS wild-type state predicts survival and is associated to early radiological response in metastatic colorectal cancer treated with cetuximab. Ann Oncol 2008;19:508.
14. Loupakis F, Pollina L, Stasi I, et al. PTEN expression and KRAS mutations on primary tumors and metastases in the prediction of benefit from cetuximab plus irinotecan for patients with metastatic colorectal cancer. J Clin Oncol 2009;27:2622.
15. Benvenuti S, Sartore-Bianchi A, Di Nicolantonio F, et al. Oncogenic activation of the RAS/RAF signaling pathway impairs the response of metastatic colorectal cancers to antiepidermal growth factor receptor antibody therapies. Cancer Res 2007;67:2643.
16. Severin GW, Engle JW, Barnhart TE, Nickles RJ. Zr-89 radiochemistry for positron emission tomography. Med Chem 2012;7:389–394.
17. Schechter NR, Chechter NR, Wendt RE, et al. Radiation dosimetry of ^{99m}Tc-labeled C225 in patients with squamous cell carcinoma of the head and neck. J Nucl Med 2004;45:1683.
18. Schechter NR, Yang DJ, Azhdarinia A, et al. Assessment of epidermal growth factor receptor with ^{99m}Tc-ethylenedicysteine-C225 monoclonal antibody. Anticancer Drugs 2003;14:49.
19. Evans HL, Nguyen Q, Carroll LS, et al. A bioorthogonal 68 Ga-labeling strategy is alive rapid in imaging. Chem Commun 2014;50:9557.
20. Zeng D, Guo Y, White AG, et al. Comparison of conjugation strategies of cross-bridged macrocyclic chelators with cetuximab for copper-64 radiolabeling and PET imaging of EGFR in colorectal tumor-bearing mice. Mol Pharm 2014;11:3980.
21. Ping LW, Meyer LA, Capretto DA, et al. Receptor-binding, biodistribution, and metabolism studies of ^{64}Cu-DOTA-cetuximab, a PET-imaging agent for epidermal growth-factor receptor-positive tumors. Cancer Biother Radiopharm 2008;23:158.
22. Cai W, Chen K, He L, et al. Quantitative PET of EGFR expression in xenograft-bearing mice using ^{64}Cu-labeled cetuximab, a chimeric anti-EGFR monoclonal antibody. Eur J Nucl Med Mol Imaging 2007;34:850.
23. Niu G, Li Z, Xie J, et al. PET of EGFR antibody distribution in head and neck squamous cell carcinoma models. J Nucl Med 2009;50:1116.
24. Anderson CJ, Ferdani R. Copper-64 radiopharmaceuticals for PET imaging of cancer: Advances in preclinical and clinical research. Cancer Biother Radiopharm 2009;4:379.
25. Verel I, Visser GWM, Boerman OC, et al. Long-lived positron emitters zirconium-89 and iodine-124 for scouting of therapeutic radioimmunoconjugates with PET. Cancer Biother Radiopharm 2014;18:655.
26. Pentlow KS, Graham MC, Lambrecht RM, et al. Quantitative imaging of iodine-124 with PET. J Nucl Med 1996;37:1557.

27. Lee FT, O'Keefe GJ, Gan HK, et al. Immuno-PET quantitation of de2–de7 epidermal growth factor receptor expression in glioma using ^{124}I-IMP-R4-labeled antibody ch806. J Nucl Med 2010;51:967.
28. Cheng C, Ho AS. SPECT imaging evaluation of 111indium-chelated cetuximab for diagnosing EGFR-positive tumor in a HCT15-induced colorectal xenograft. Gastroenterology 2017;152:551.
29. Shih YH, Peng CL, Lee SY, et al. 111In-cetuximab as a diagnostic agent by accessible epidermal growth factor (EGF) receptor targeting in human metastatic colorectal carcinoma. Oncotarget 2015;6:16601.
30. Van Dijk LK, Hoeben BAW, Kaanders JHAM, et al. Imaging of epidermal growth factor receptor expression in head and neck cancer with SPECT/CT and 111In-labeled cetuximab-F(ab′)2. J Nucl Med 2013;54:2118.
31. Misri R, Saatchi K, Isri R, et al. Evaluation of (111)In labeled antibodies for SPECT imaging of mesothelin expressing tumors. Nucl Med Biol 2011;38:885.
32. Huhtala T, Laakkonen P, Sallinen H, et al. In vivo SPECT/CT imaging of human orthotopic ovarian carcinoma xenografts with 111In-labeled monoclonal antibodies. Nucl Med Biol 2010;37:957.
33. Divgi CR, Welt S, Kris M, et al. Phase I and imaging trial of indium-111 labeled anti-epidermal growth factor receptor monoclonal antibody 225 in patients with squamous cell lung carcinoma. J Natl Cancer Inst 1991;83:97.
34. Zhang Y, Hong H, Cai W. PET tracers based on Zirconium-89. Curr Radiopharm 2011;2:131.
35. Jauw YW, Menke-van der Houven van Oordt CW, Hoekstra OS, et al. Immuno-positron emission tomography with zirconium-89-labeled monoclonal antibodies in oncology: What can we learn from initial clinical trials? Front Pharmacol 2016;7:131.
36. Perk LR, Vosjan MJ, Visser GW, et al. P-isothiocyanatobenzyl-desferrioxamine: A new bifunctional chelate for facile radiolabeling of monoclonal antibodies with zirconium-89 for immuno-PET imaging. Eur J Nucl Med Mol Imaging 2010;37:250.
37. Van Loon J, Even AJG, Aerts HJW, et al. PET imaging of zirconium-89 labelled cetuximab: A phase I trial in patients with head and neck and lung cancer. Radiother Oncol 2016; 11:1016.
38. Even AJG, Hamming-Vrieze O, van Elmpt W, et al. Quantitative assessment of Zirconium-89 labeled cetuximab using PET/CT imaging in patients with advanced head and neck cancer: A theragnostic approach. Cancer Data 2017;83:1.
39. Vosjan MJWD, Perk LR, Visser GWM, et al. Conjugation and radiolabeling of monoclonal antibodies with zirconium-89 for PET imaging using the bifunctional chelate p-isothiocyanatobenzyl-desferrioxamine. Nat Protoc 2010;5:739.
40. van de Watering FCJ, Rijpkema M, Perk L, et al. Zirconium-89 labeled antibodies: A new tool for molecular imaging in cancer patients. Biomed Res Int 2014;14:1.
41. Nayak TK, Brechbiel MW. Radioimmunoimaging with longer-lived positron-emitting radionuclides: Potentials and challenges. Bioconjug Chem 2009;5:825.
42. Verel I, Visser GWM, Boellaard R, et al. ^{89}Zr immuno-PET: Comprehensive procedures for the production of ^{89}Zr-labeled monoclonal antibodies. J Nucl Med 2003;44:1271.
43. Deri MA, Zeglis BM, Francesconi LC, et al. PET imaging with 89Zr: From radiochemistry to the clinic. Nucl Med Biol 2013; 40:3.
44. Aerts HJ, Dubois L, Perk L, et al. Disparity between in vivo EGFR expression and (89)Zr-labeled cetuximab uptake assessed with PET. J Nucl Med 2009;50:123.
45. Perk LR, Visser GW, Vosjan MJ, et al. ^{89}Zr as a PET surrogate radioisotope for scouting biodistribution of the therapeutic radiometals ^{90}Y and ^{177}Lu in tumor-bearing nude mice after coupling to the internalizing antibody Cetuximab. J Nucl Med 2005;46:1898.
46. Menke-Van CW, Gootjes EC, Huisman MC, et al. ^{89}Zr-cetuximab PET imaging in patients with advanced colorectal cancer. Oncotarget 2015;6:30384.
47. Meijs WE, Herscheid JDM, Haisma HJ, et al. Evaluation of desferal as a bifunctional chelating agent for labeling antibodies with Zr-89. Appl Radiat Isot 1992;43:1443.
48. Wooten L, Madrid E, Schweitzer GD, et al. Routine production of ^{89}Zr using an automated module. Appl Sci 2013;3:593.
49. van Dongen GA, Visser GW, Lub-De Hooge MN, et al. Immuno-PET: A navigator in monoclonal antibody development and applications. Oncologist 2007;12:1379.
50. Natarajan A, Habte F, Gambhir SS. Development of a novel long-lived ImmunoPET tracer for monitoring lymphoma therapy in a humanized transgenic mouse model. Bioconjug Chem 2012;6:1221.
51. Millenic DE, Wong KJ, Baidoo KE, et al. Cetuximab: Preclinical evaluation of a monoclonal antibody targeting EGFR for radioimmunodiagnostic and radioimmunotherapeutic applications. Cancer Biother Radiopharm 2008;23:619.
52. Queern SL, Aweda TA, Massicano AVF, et al. Production of Zr-89 using sputtered yttrium coin targets 89Zr using sputtered yttrium coin targets. Nucl Med Biol 2017;50:11.
53. Oliveira JSR. Identificação de novos biomarcadores preditivos da resposta às terapias anti-EGFR em tumores sólidos: ênfase em tumores de cabeça e pescoço. (Doctoral dissertation, São Paulo, Brazil: Fundação Pio XII–Hospital de Câncer de Barretos). 2016.
54. Okada Y, Kimura T, Nakagawa T, et al. EGFR downregulation after anti-EGFR therapy predicts the antitumor effect in colorectal cancer. Mol Cancer Res 2017;16:1.
55. Tao X, Lu Y, Qiu S, et al. AP1G1 is involved in cetuximab-mediated downregulation of ASCT2-EGFR complex and sensitization of human head and neck squamous cell carcinoma cells to ROS-induced apoptosis. Cancer Lett 2017;408:33.
56. Sequist LV, Waltman BA, Dias-Santagata D, et al. Genotypic and histological evolution of lung cancers acquiring resistance to EGFR inhibitors. Sci Transl Med 2011;3:15.
57. Kani K, Garri C, Tiemann K, et al. JUN-mediated downregulation of EGFR signaling is associated with resistance to gefitinib in EGFR-mutant NSCLC cell lines. Mol Cancer Ther 2017;16:1645.
58. Manole S, Richards EJ, Meyer AS. JNK pathway activation modulates acquired resistance to EGFR/HER2-targeted therapies. Cancer Res 2016;76:5219.
59. Benedetto R. [89]Zr-Imuno-PET/[111] In-Imuno-SPECT: desenvolvimento radiofarmacêutico de agentes de imagem molecular para receptores EGF. (Doctoral dissertation, São Paulo, Brazil: Instituto de Pesquisas Energéticas e Nucleares). 2017.
60. Chang AJ, De Silva RA, Lapi SE. Development and characterization of 89 Zr-labeled panitumumab for immuno–positron emission tomographic imaging of the epidermal growth factor receptor. Mol Imaging 2013;88:12117.
61. England CG. Preclinical pharmacokinetics and biodistribution studies of 89Zr-labeled pembrolizumab. J Nucl Med 2017;1:162.